

## Article

# Hydrothermal Alteration and Element Migration Patterns in the Zhangjiawu Uranium Deposit, Northern Zhejiang Province, China

Wengao Zhang <sup>1,\*</sup> , Bo Wang <sup>2</sup>, Yifei Tang <sup>1,3</sup>, Wei Li <sup>1,4</sup>, Xiaohu Wang <sup>1</sup> , Zhenghua Xu <sup>5</sup>, Xun Liu <sup>5</sup> and Zhengle Chen <sup>1</sup> 

<sup>1</sup> Key Laboratory of Paleomagnetism and Tectonic Reconstruction, Ministry of Natural Resources, Institute of Geomechanics, Chinese Academy of Geological Sciences, Beijing 100081, China

<sup>2</sup> No. 280 Institute of Nuclear Industry, Guanghan 618300, China

<sup>3</sup> Institute of Geologic Survey, China University of Geosciences, Wuhan 430074, China

<sup>4</sup> School of Earth Science and Resources, Chang'an University, Xi'an 710054, China

<sup>5</sup> No. 262 Geological Party of Zhejiang Nuclear Industry Corp., Huzhou 313000, China

\* Correspondence: zhangwengao@mail.cgs.gov.cn

**Abstract:** The Zhangjiawu uranium deposit is the largest volcanic rock-type uranium deposit in the northern Zhejiang Province, China. The deposit has developed hydrothermal alteration, with obvious alternating zoning phenomena from the mineralized center to the fresh surrounding rocks. Based on detailed field and petrographic observations of typical ore bodies, the uranium mineralized section of the Zhangjiawu uranium deposit was divided into mineralized central, ore-side alteration, near-ore alteration and far-ore alteration zones, whose hydrothermal alteration intensity decreases sequentially. Using the standardized Isocon diagram method, the results show that CaO, MgO, Na<sub>2</sub>O, P<sub>2</sub>O<sub>5</sub>, LOI, Zn, Co, Cu, Pb and heavy rare earth elements (HREE) show gain during uranium mineralization, while K<sub>2</sub>O, Cs, Rb and Tl show loss, which is consistent with the development of hematite mineralization, sodic feldsparization and carbonation in the mine area. A negative correlation of MnO and MgO in the alteration zone indicates a possible elemental convective equilibrium migration mode in the ore zone. The migration mechanism of the elements indicates that the migration of P<sub>2</sub>O<sub>5</sub> and HREE indicates the deep source nature of the mineralizing fluids, and that alteration can lead to a reduction in the activity of uranyl complexes, the formation of a reducing environment and a neutral to weak alkaline environment favorable for uranium precipitation, which can lead to uranium precipitation and enrichment of mineralization. The study of hydrothermal alteration and elemental migration patterns of the deposit provides supporting evidence for a better understanding of the process of uranium mineralization in Zhangjiawu, and also provides a basis for the next step of mineral search and exploration.

**Keywords:** alteration zonation; mass balance calculation; elemental migration; Zhangjiawu uranium mine; Zhejiang Province



**Citation:** Zhang, W.; Wang, B.; Tang, Y.; Li, W.; Wang, X.; Xu, Z.; Liu, X.; Chen, Z. Hydrothermal Alteration and Element Migration Patterns in the Zhangjiawu Uranium Deposit, Northern Zhejiang Province, China. *Minerals* **2023**, *13*, 335. <https://doi.org/10.3390/min13030335>

Academic Editor: Mariko Nagashima

Received: 10 November 2022

Revised: 22 February 2023

Accepted: 23 February 2023

Published: 27 February 2023



**Copyright:** © 2023 by the authors. Licensee MDPI, Basel, Switzerland. This article is an open access article distributed under the terms and conditions of the Creative Commons Attribution (CC BY) license (<https://creativecommons.org/licenses/by/4.0/>).

## 1. Introduction

Hydrothermal fluid itself or hydrothermal fluid circulation causes physicochemical changes in the rocks through which it circulates, which is known as “hydrothermal alteration”. The type and characteristics of hydrothermal alteration depend on the source, nature, chemical composition, temperature, pressure and other physicochemical conditions of the hydrothermal fluid, as well as the lithology, structure and composition of the surrounding rock [1]. The process of hydrothermal alteration inevitably leads to the migration of elements. Having a precise definition of the type and extent of the migrating geochemical components is a prerequisite for understanding hydrothermal alteration [2,3]. Geochemical methods have been used to characterize the assemblages of minerals involved in the alteration process of hydrothermal deposits and to study the intensity of hydrothermal alteration and elemental migration patterns in order to reveal the relationship between

various alteration processes and mineralization [4–7]. Understanding the process of hydrothermal alteration is also of obvious significance for mineral exploration, as the extent of hydrothermal alteration is usually larger than the distribution of ore bodies [8].

The mass balance calculation is a method used to study the migration of arbitrary components in and out of hydrothermal alteration processes. The idea of mass balance calculation was first proposed independently by Akella (1966) and Gresens (1967), who derived the famous Gresens formula based on his basic idea and established the corresponding graphical method, which laid the foundation of mass balance calculation research [9,10]. This method is based on the estimation of the tendency (migration in or out) and extent of migration of any component (generally attributed to oxides or elements) during the opening of the system based on the substance content of the sample before and after the opening of the system [10–12]. For any component, the mass before migration of the substance is equal to the sum of the mass after migration of the substance and the migrated mass. The mass of a component that undergoes migration can be inferred from the difference between the mass of that component before and after migration occurs.

The four major uranium ore types, volcanic, granitic, sandstone and carbon-silica mudstone, have all been found in the Zhejiang Province, China. The Zhangjiawu uranium deposit is the largest volcanic-type uranium deposit in northern Zhejiang. A series of results has been obtained from previous studies on these ore bodies, mineralized zones and alteration types of the surrounding rocks of the Zhangjiawu uranium deposit [13,14]. Previous studies on the alteration of the surrounding rocks of the Zhangjiawu uranium deposit have mainly focused on the zoning of the alteration of the surrounding rocks, the combination of alternating minerals and the classification of phases [14,15], but less research has been conducted on the migration patterns of elements in different mineralized alteration zones. This has limited the understanding of hydrothermal alteration mechanisms and mineral migration, as well as of precipitation mechanisms. Therefore, based on detailed field, petrographic, and mineralogical work, the geochemical characterization of main, trace and rare earth elements (REEs) was carried out on representative rock and ore samples from the mineralized alteration profiles using the mass balance calculation method (standardized Isocon diagram method) fitted by Guo et al. [2,16]. The transferring pattern of alteration zone components of Zhangjiawu uranium ore was studied in an attempt to explore the source of mineralized material and the transferring pattern of elements. By understanding the metallogenic characteristics and mineralization mechanism of the Zhangjiawu uranium deposit, we provide a basis for the mineralization pattern and uranium search in the mining area.

## 2. Geological Setting

The northern part of Zhejiang is located at the southeastern margin of the Yangtze plate (Figure 1A). In the zoning of uranium mineralization in China, the northern part of Zhejiang is located in the Tianmu Mountain Volcanic Uranium Prospect Zone, which has large potential for the discovery of uranium ore [17–19]. The main outcrops in the area are the Early Paleozoic (Silurian), a small part are Late Paleozoic (Devonian–Carboniferous) and Mesozoic (Cretaceous), and numerous are Cenozoic. The Middle and Lower Silurian are a set of shallow marine siliceous, carbonaceous, muddy and mud-bearing clastic strata, the Upper Devonian is a coastal-phase quartz conglomerate, and the Upper Carboniferous is a terrace-phase carbonate formation; volcanic activity in the area was most active during the Mesozoic period, and three phases of medium-acidic and highly alkaline volcanic rocks (quartz crinoid, crinoid, clastic and rhyolitic rocks) were formed over short time intervals. The strata are generally unconformable and overlain by Paleozoic strata. These fractures constrained the Mesozoic medium-acidic magmatic intrusion in northern Zhejiang [20,21].

The Zhangjiawu uranium mine contains the largest uranium deposit in the northern Zhejiang Province. The stratigraphy of the Silurian marine sedimentary rocks is exposed on the west side of the Huzhou-Xuechuan Fault, while the stratigraphy on the east side is represented mainly by volcanic rocks from the lower to middle part of the Lower Cretaceous Huangjian Group (Figure 2). The second lithological layer ( $K_1h^{1-2}$ ) of the lower part of the Huangjian Group, the third lithological layer ( $K_1h^{1-3}$ ) of dacitic clastic lava, the lower part of the first lithological layer of the middle part ( $K_1h^{2-1a}$ ) of rhyolitic clastic tuff and the lower part of the third lithological layer of the middle part ( $K_1h^{2-3a}$ ) of striped spherical rhyolite have high uranium content,  $w(U)$  ( $6.20 \times 10^{-6}$  to  $9.25 \times 10^{-6}$ ). The average uranium content of normal rhyolite is  $5-6 \times 10^{-6}$  [15].  $K_1h^{2-1a}$  and  $K_1h^{2-3a}$  are the main mineral-bearing lithologies in this area. The lower part of the third lithologic layer ( $K_1h^{2-3a}$ ) in the middle section of the Huangjian Formation is brownish-purple and grayish-purple in color, with a porphyritic structure, spherical and banded structure, and is in gradual contact with the second lithologic layer, which has obvious rhyolite bands and is the main ore-bearing layer of the Zhangjiawu uranium deposit.

The NE-NNE trending faults are well developed in the Zhangjiawu mining area, which is basically consistent with the regional fault structures (Figure 2). The  $F_1$  fracture is located in the central part of the mine area, with a strike of about  $10^\circ$  to  $20^\circ$ , SE trending, and a dip of  $80^\circ$  to  $85^\circ$ . This is a normal fault, which is the western boundary of the Cretaceous volcanic basin. The  $F_{10}$  fracture is located in the central part of the mine area, with a fracture width of 1–1.5 m, strike  $25^\circ-35^\circ$ , and dip SE  $70^\circ-85^\circ$  (Figure 3d). The early tectonic activity formed weakly reddened fractured rocks in  $F_{10}$  fracture, while late tectonic activity formed some tectonic breccias, a few siliceous veins and carbonate veins filled in the fractures in a mesh. The NW fractures are densely distributed in the mine area and are small in scale, and interrupt the fracture groups formed first, which are mostly positive faults. Some arc-shaped (fracture) structures also formed near the caldera due to volcanic activity, which are distributed in a radial pattern on the southern side of the Shimenshan caldera in the mine area, with a steep dip angle of about  $80^\circ$ . Industrial-quality uranium ore bodies are found in their lower plates, which are not visible on the surface due to their thick cover.

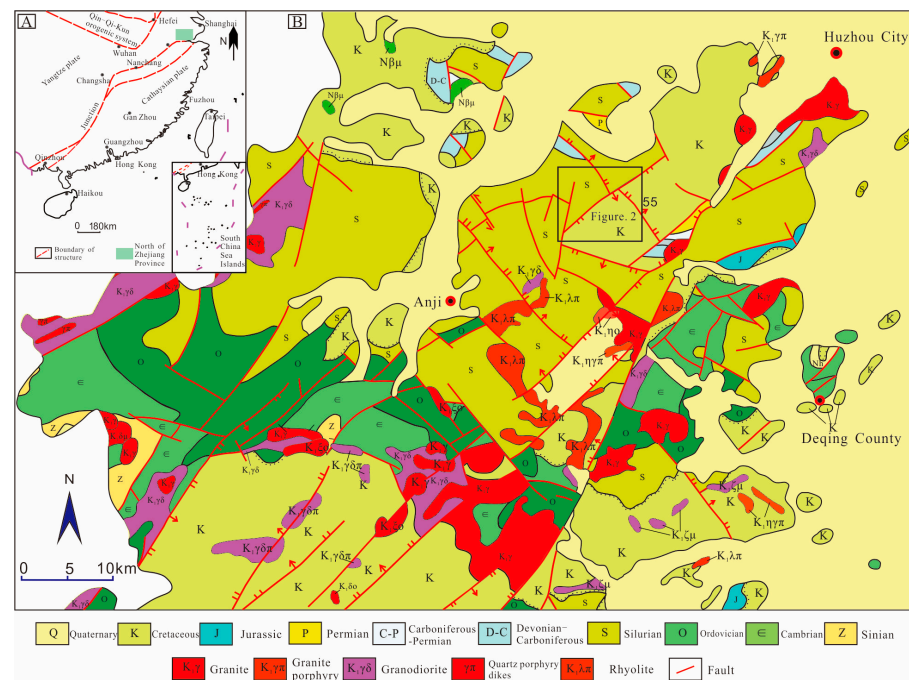
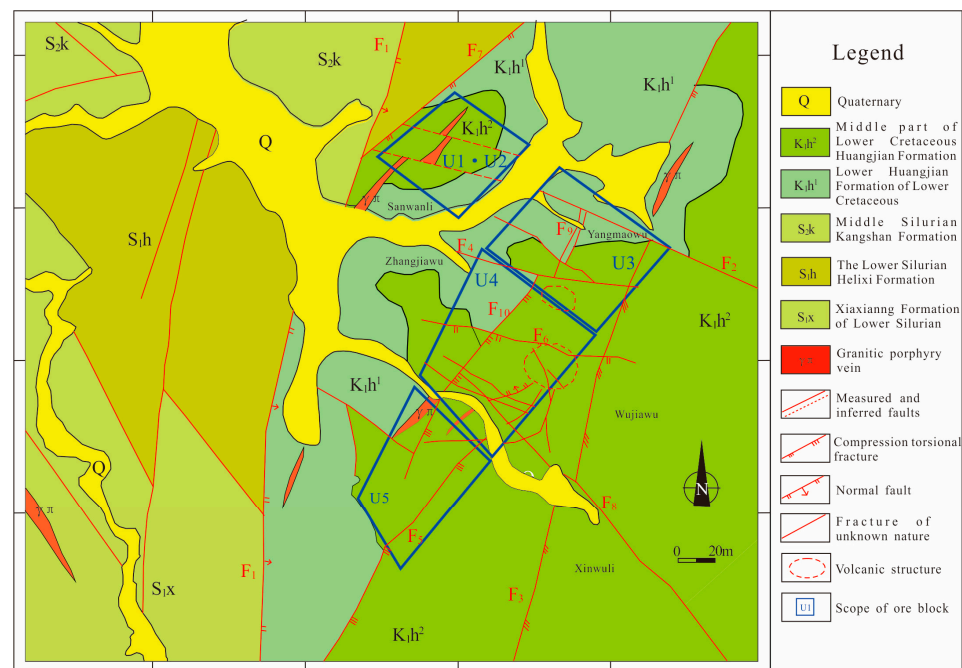
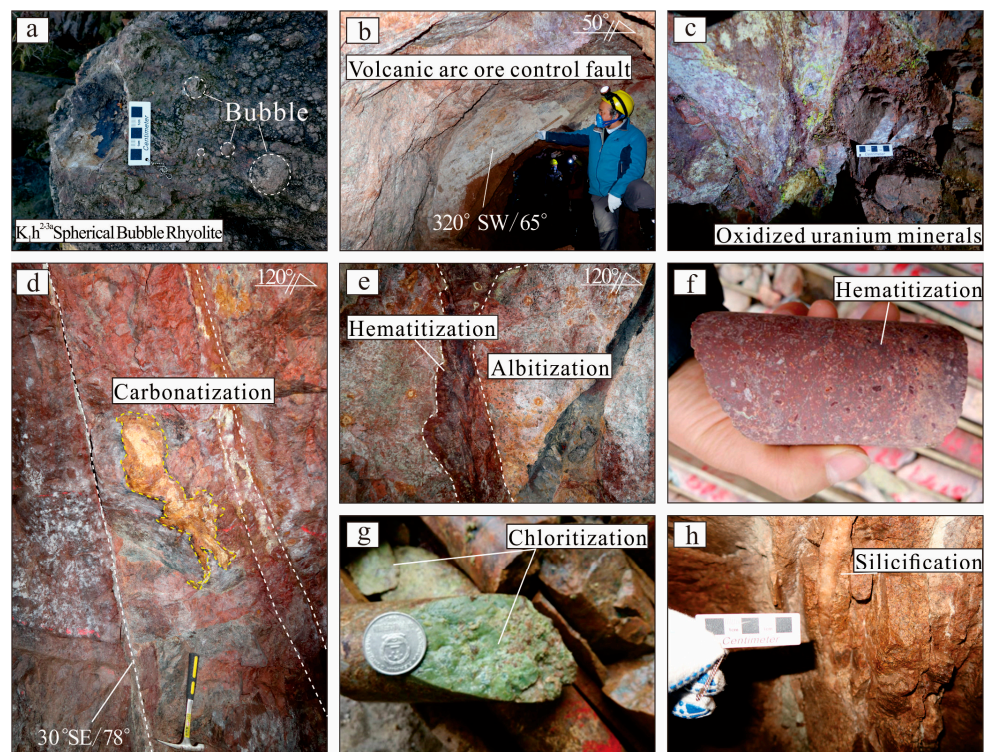


Figure 1. (A) Geotectonic position and (B) a regional geological sketch in northern Zhejiang Province (according to ref. [22]).



**Figure 2.** Geological sketch map of the Zhangjiawu mining area in northern Zhejiang Province, China (U1, U2, U3, U4 and U5 refers to different uranium sections respectively).



**Figure 3.** Orebody occurrence characteristics and alteration of the Zhangjiawu uranium deposit, Zhejiang Province, China; (a) Lower part of the third lithologic layer ( $K_1h^{2-3a}$ ) of the unaltered Upper Cretaceous Huangjian Formation; (b) NW-trending volcanic arc ore-bearing fractures; (c) oxidation of tetravalent uranium minerals to brightly colored hexavalent uranium minerals; (d) F10 compression-torsional ore-control fractures with hematite and carbonatization near the fractures; (e) hematite mineralization superimposed along the fractures on early sodic feldsparization; (f) hematite mineralization; (g) chlorite mineralization; (h) silicification seen further away from the center of mineralization.

### 3. Sample Characterization and Testing

#### 3.1. Sampling and Alteration Zonation Characteristics

Field geological investigations have shown that the degree of mineralized alteration and alteration type of the rocks exhibit certain zoning phenomena from the fracture structure outwards to the newer fresh surrounding rocks (which lack hydrothermal alteration). In this paper, the altered rocks are divided into four gradual transitional alteration zones, namely the mineralized central (A), adjacent alteration (B), near alteration (C) and far alteration zones (D), based on the characteristics of the altered rocks. As a comparison, we also collected fresh rhyolite (E). Representative samples are collected for each rock type. These are described below as follows.

Mineralized central zone (A): the most strongly altered sample of ore from the Zhangjiawu uranium deposit. The ore is red in color and relatively fragmented (Figure 4a), with strong hematite, chlorite, carbonate and clay mineralization, and fine-grained pyrite can be seen in the margins suffering from dissolution; potassium feldspar has undergone strong modification and has an earthy surface (Figure 4b,c).

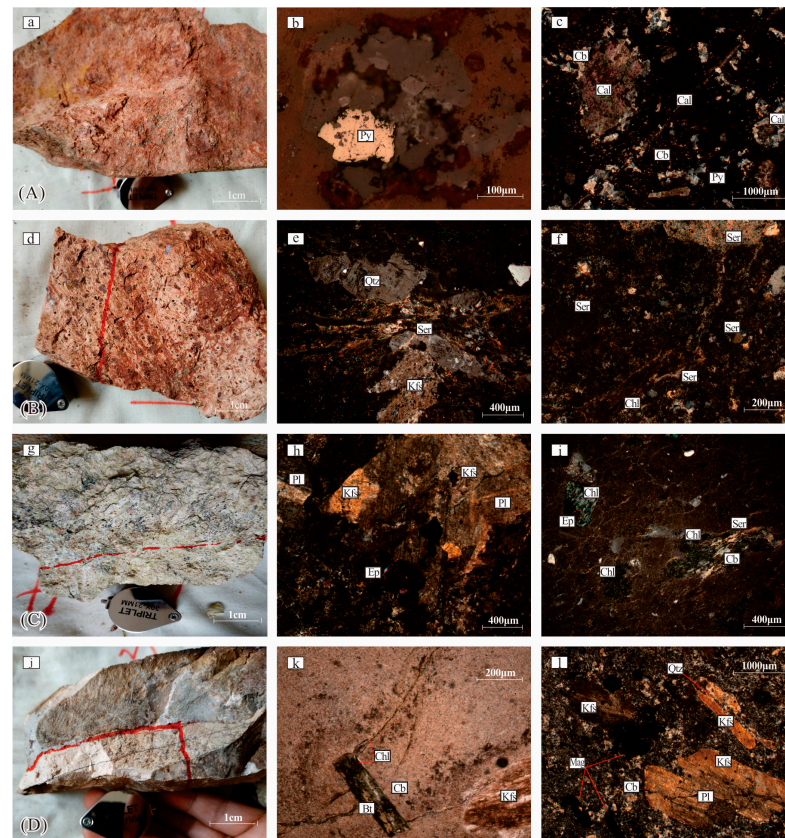


**Figure 4.** Rock characteristics of four alteration zones: (A) mineralization center; the most strongly altered sample of ore from the Zhangjiawu uranium deposit. The ore is red in color and relatively fragmented (a), with strong hematite, chlorite, carbonate and clay mineralization, and fine-grained pyrite can be seen in the margins suffering from dissolution; potassium feldspar has undergone strong modification and has an earthy surface (b,c); (B) adjacent alteration zone: the rock is reddish in color (d), with strong sericitization, chloritization and clayification, and strong hematite mineralization in places (e,f); (C) near alteration zone: the rocks are grayish-white-light green (g), with strong chloritization, sericitization, sodic feldspar and carbonatization, and chloritization of black mica is visible (h,i); (D) far alteration zone: the rocks are light red (j), with mainly sodic feldsparization, chloritization of black mica, carbonatization and strong modification of potassium feldspar (k,l). Py—pyrite; Qtz—quartz; Chl—chlorite; Ep—chlorite; Pl—plagioclase; Ser—sericite—sericite—calcite; Kfs—potassium feldspar; Bt—black mica; Mag—magnetite.

Adjacent alteration zone (B): the rock is reddish in color (Figure 4d), with strong sericitization, chloritization and clayification and strong hematite mineralization in places (Figure 4e,f).

Near alteration zone (C): the rocks are grayish-white-light green (Figure 4g), with strong chloritization, sericitization, sodic feldspar and carbonatization; chloritization of black mica is visible (Figure 4h,i).

Far alteration zone (D): the rocks are light red (Figure 4j), with mainly sodic feldsparization, chloritization of black mica, carbonatization and strong modification of potassium feldspar (Figure 4k,l).

Fresh rhyolite (E): The lithology is striped bubble rhyolite, brownish purple and grayish purple, porphyritic structure, spherical and striped structure (Figure 3a).

### 3.2. Sample Testing

Based on the above detailed petrographic and mineralogical observations, representative rock and ore samples were crushed and ground to 200 mesh and sent to Wuhan Sample Solution Analytical Technology Co., Wuhan, China, for analysis. The main elements were analyzed with a ZSX Primus II wavelength dispersive X-ray fluorescence spectrometer (XRF), Rigaku Corp., Tokyo, Japan, with a relative standard deviation (RSD) of <2%. The detailed analysis process can be found in GB/T 14506.14-2010 "Methods for Chemical Analysis of Silicate rocks". An inductively coupled plasma mass spectrometer (ICP-MS), model Agilent 7700e, Agilent Tech., Palo Alto, CA, USA, was used for the analysis of trace elements and REEs, with a relative deviation (RD) < 10%. The test method was based on DZ/T 0223-2001 "Inductively coupled plasma mass spectrometry analysis Method General Principles". The results are presented in Tables 1–3. Raw data: unprocessed data detected by the instrument. Standardization factor calculation method: inactive component content of sample Zone A/inactive component content of other alteration samples. Standardized data: data processed with standardized coefficients. Projection data: data after scaling factor processing. Migration rate: represents the migration pattern of the element during the alteration process: "-" means move out; vice versa for move in. LOI: represents the amount of rock burned during the test.  $OI = Fe_2O_3 / (Fe_2O_3 + FeO)$ . Characteristic value (Table 4): indicative values derived from relevant calculations.

**Table 1.** Major element content (wt %) and data processing results of ore-fresh rock zoning rocks in the Zhangjiawu uranium deposit, Zhejiang Province, China.

|                 | Sub-Zone | SiO <sub>2</sub> | TiO <sub>2</sub> | Al <sub>2</sub> O <sub>3</sub> | TFe <sub>2</sub> O <sub>3</sub> | FeO   | MnO   | MgO   | CaO   | Na <sub>2</sub> O | K <sub>2</sub> O | P <sub>2</sub> O <sub>5</sub> | LOI  | Standardization Factor |
|-----------------|----------|------------------|------------------|--------------------------------|---------------------------------|-------|-------|-------|-------|-------------------|------------------|-------------------------------|------|------------------------|
| Raw data        | Zone A   | 69.8             | 0.38             | 13.8                           | 2.11                            | 0.50  | 0.06  | 0.44  | 1.63  | 7.04              | 1.49             | 0.10                          | 3.10 | 1.00                   |
|                 | Zone B   | 69.3             | 0.37             | 13.8                           | 2.73                            | 0.42  | 0.05  | 0.36  | 1.47  | 4.99              | 4.48             | 0.10                          | 1.71 | 1.04                   |
|                 | Zone C   | 71.1             | 0.36             | 13.9                           | 3.69                            | 0.08  | 0.05  | 0.14  | 0.29  | 5.12              | 3.85             | 0.09                          | 1.13 | 1.05                   |
|                 | Zone D   | 72.1             | 0.38             | 13.8                           | 2.41                            | 0.06  | 0.04  | 0.13  | 0.23  | 4.23              | 5.13             | 0.09                          | 1.01 | 1.00                   |
|                 | Zone E   | 72.9             | 0.36             | 14.4                           | 1.30                            | 0.58  | 0.05  | 0.15  | 0.25  | 3.49              | 6.24             | 0.09                          | 0.59 |                        |
| Standardization | Zone A   | 69.8             | 0.38             | 13.8                           | 2.11                            | 0.50  | 0.06  | 0.44  | 1.63  | 7.04              | 1.49             | 0.10                          | 3.10 |                        |
|                 | Zone B   | 72.1             | 0.38             | 14.3                           | 2.84                            | 0.44  | 0.05  | 0.38  | 1.53  | 5.20              | 4.66             | 0.10                          | 1.78 |                        |
|                 | Zone C   | 74.4             | 0.38             | 14.5                           | 3.87                            | 0.08  | 0.05  | 0.14  | 0.30  | 5.36              | 4.03             | 0.09                          | 1.18 |                        |
|                 | Zone D   | 72.1             | 0.38             | 13.8                           | 2.41                            | 0.06  | 0.04  | 0.13  | 0.23  | 4.23              | 5.13             | 0.09                          | 1.01 |                        |
| Projection data | Zone A   | 33.5             | 5.25             | 38.2                           | 40.5                            | 17.2  | 64.0  | 45.4  | 48.1  | 60.5              | 14.2             | 52.2                          | 52.4 |                        |
|                 | Zone B   | 34.6             | 5.25             | 39.8                           | 54.5                            | 15.0  | 47.8  | 38.6  | 45.3  | 44.6              | 44.8             | 52.7                          | 30.2 |                        |
|                 | Zone C   | 35.7             | 5.25             | 40.3                           | 74.2                            | 2.89  | 51.3  | 14.5  | 8.87  | 46.0              | 38.7             | 46.0                          | 20.0 |                        |
|                 | Zone D   | 34.5             | 5.30             | 38.3                           | 46.3                            | 2.07  | 42.0  | 13.7  | 6.76  | 36.3              | 49.3             | 46.5                          | 17.1 |                        |
|                 | Zone E   | 35.0             | 5.00             | 40.0                           | 25.0                            | 20.0  | 50.0  | 15.0  | 7.50  | 30.0              | 60.0             | 45.0                          | 10.0 |                        |
|                 | Scaling  | 0.48             | 13.8             | 2.77                           | 19.2                            | 34.4  | 1000  | 102   | 29.5  | 8.59              | 9.61             | 517                           | 16.9 |                        |
| Migration rate  | Zone A   | −0.09            | −0.01            | −0.09                          | 0.54                            | −0.18 | 0.21  | 1.87  | 5.08  | 0.91              | −0.77            | 0.10                          | 3.97 |                        |
|                 | Zone B   | −0.06            | 0.00             | −0.05                          | 1.08                            | −0.28 | −0.09 | 1.45  | 4.76  | 0.42              | −0.29            | 0.12                          | 1.88 |                        |
|                 | Zone C   | −0.03            | 0.00             | −0.04                          | 1.83                            | −0.86 | −0.02 | −0.08 | 0.13  | 0.46              | −0.38            | −0.03                         | 0.91 |                        |
|                 | Zone D   | −0.07            | 0.00             | −0.10                          | 0.75                            | −0.90 | −0.21 | −0.13 | −0.15 | 0.14              | −0.23            | −0.02                         | 0.62 |                        |

**Table 2.** Trace element content ( $\times 10^{-6}$ ) and data processing results of ore-fresh rock zoning rocks in the Zhangjiawu uranium deposit, Zhejiang Province, China.

|                 | Sub-Banding | Li    | Be    | Sc    | V     | Cr    | Co    | Ni    | Cu    | Zn     | Ga    | Rb     | Sr     | Standardization Factor |
|-----------------|-------------|-------|-------|-------|-------|-------|-------|-------|-------|--------|-------|--------|--------|------------------------|
| Raw data        | Zone A      | 2.41  | 2.25  | 4.89  | 11.47 | 1.40  | 3.79  | 1.16  | 2.81  | 146.46 | 15.96 | 56.50  | 89.10  | 1.00                   |
|                 | Zone B      | 1.34  | 1.95  | 5.42  | 19.57 | 1.37  | 2.17  | 0.91  | 1.72  | 28.78  | 16.15 | 156.74 | 137.02 | 1.04                   |
|                 | Zone C      | 4.25  | 2.96  | 4.85  | 14.88 | 1.50  | 2.11  | 0.98  | 5.23  | 48.09  | 15.90 | 133.51 | 97.82  | 1.05                   |
|                 | Zone D      | 3.45  | 2.29  | 4.88  | 15.5  | 1.84  | 1.75  | 0.86  | 1.73  | 28.0   | 15.3  | 176    | 101    | 1.00                   |
|                 | E-zone      | 3.02  | 2.49  | 5.12  | 15.2  | 1.31  | 2.17  | 1.09  | 1.74  | 28.9   | 16.4  | 184    | 118    |                        |
| Standardization | Zone A      | 2.41  | 2.25  | 4.89  | 11.4  | 1.40  | 3.79  | 1.16  | 2.81  | 146    | 15.9  | 56.5   | 89     |                        |
|                 | Zone B      | 1.40  | 2.03  | 5.64  | 20.3  | 1.43  | 2.26  | 0.95  | 1.79  | 29.9   | 16.8  | 163    | 142    |                        |
|                 | Zone C      | 4.45  | 3.09  | 5.08  | 15.5  | 1.57  | 2.21  | 1.03  | 5.48  | 50.3   | 16.6  | 139    | 102    |                        |
|                 | Zone D      | 3.45  | 2.29  | 4.88  | 15.5  | 1.84  | 1.75  | 0.86  | 1.73  | 28.0   | 15.3  | 176    | 101    |                        |
| Projection data | Zone A      | 3.98  | 49.5  | 47.7  | 11.3  | 48.3  | 39.2  | 56.2  | 16.1  | 63.3   | 29.0  | 17.6   | 24.5   |                        |
|                 | Zone B      | 2.31  | 44.8  | 55.0  | 20.1  | 49.0  | 23.4  | 45.6  | 10.2  | 12.9   | 30.5  | 50.9   | 39.2   |                        |
|                 | Zone C      | 7.36  | 68.2  | 49.5  | 15.3  | 54.0  | 22.8  | 49.7  | 31.4  | 21.7   | 30.2  | 43.6   | 28.1   |                        |
|                 | Zone D      | 5.70  | 50.5  | 47.6  | 15.3  | 63.3  | 18.1  | 41.4  | 9.92  | 12.1   | 27.9  | 55.1   | 27.7   |                        |
|                 | Zone E      | 5.00  | 55.0  | 50.0  | 15.0  | 45.0  | 22.5  | 52.5  | 10.0  | 12.5   | 30.0  | 57.5   | 32.5   |                        |
|                 | Scaling     | 1.66  | 22.0  | 9.76  | 0.99  | 34.4  | 10.3  | 48.3  | 5.74  | 0.43   | 1.82  | 0.31   | 0.27   |                        |
| Migration rate  | Zone A      | -0.25 | -0.15 | -0.10 | -0.29 | 0.02  | 0.65  | 0.01  | 0.53  | 3.80   | -0.08 | -0.71  | -0.29  |                        |
|                 | Zone B      | -0.56 | -0.22 | 0.05  | 0.28  | 0.04  | -0.01 | -0.17 | -0.02 | -0.01  | -0.03 | -0.16  | 0.15   |                        |
|                 | Zone C      | 0.40  | 0.18  | -0.06 | -0.02 | 0.14  | -0.03 | -0.10 | 1.99  | 0.66   | -0.04 | -0.28  | -0.17  |                        |
|                 | Zone D      | 0.08  | -0.13 | -0.10 | -0.04 | 0.33  | -0.24 | -0.26 | -0.06 | -0.09  | -0.12 | -0.10  | -0.19  |                        |
|                 | Sub-Banding | Y     | Zr    | Nb    | Sn    | Cs    | Ba    | Hf    | Ta    | Tl     | Pb    | Th     | U      | Standardization Factor |
| Raw data        | Zone A      | 34.9  | 257   | 20.4  | 1.44  | 1.11  | 628   | 7.09  | 1.67  | 0.40   | 35.4  | 24.7   | 276    | 1.00                   |
|                 | Zone B      | 37.1  | 271   | 19.1  | 2.00  | 1.89  | 729   | 7.34  | 1.51  | 0.98   | 23.6  | 21.7   | 93.3   | 1.04                   |
|                 | Zone C      | 25.5  | 254   | 18.9  | 1.88  | 2.06  | 762   | 6.84  | 1.48  | 0.66   | 46.7  | 22.5   | 23.5   | 1.05                   |
|                 | Zone D      | 34.5  | 248   | 20.4  | 1.63  | 2.12  | 809   | 6.82  | 1.56  | 0.88   | 18.2  | 22.7   | 9.8    | 1.00                   |
|                 | E-zone      | 31.4  | 240   | 18.8  | 1.62  | 2.23  | 767   | 6.69  | 1.57  | 0.91   | 19.3  | 23.4   | 5.6    |                        |
| Standardization | Zone A      | 34.9  | 257   | 20.4  | 1.44  | 1.11  | 628   | 7.09  | 1.67  | 0.40   | 35.4  | 24.7   | 276    |                        |
|                 | Zone B      | 38.6  | 282   | 19.9  | 2.08  | 1.97  | 759   | 7.64  | 1.57  | 1.02   | 24.6  | 22.6   | 97.1   |                        |
|                 | Zone C      | 26.7  | 266   | 19.8  | 1.97  | 2.16  | 798   | 7.17  | 1.55  | 0.69   | 48.9  | 23.5   | 24.6   |                        |
|                 | Zone D      | 34.5  | 248   | 20.4  | 1.63  | 2.12  | 809   | 6.82  | 1.56  | 0.88   | 18.2  | 22.7   | 9.87   |                        |
| Projection data | Zone A      | 38.8  | 29.4  | 51.3  | 17.7  | 8.69  | 20.5  | 39.7  | 42.6  | 26.3   | 13.7  | 44.7   | 48.6   |                        |
|                 | Zone B      | 43.0  | 32.2  | 50.1  | 25.6  | 15.4  | 24.7  | 42.8  | 40.0  | 67.1   | 9.54  | 40.9   | 17.1   |                        |
|                 | Zone C      | 29.8  | 30.4  | 49.8  | 24.2  | 16.9  | 26.0  | 40.1  | 39.6  | 45.7   | 18.9  | 42.7   | 4.34   |                        |
|                 | Zone D      | 38.4  | 28.4  | 51.3  | 20.1  | 16.6  | 26.3  | 38.2  | 39.8  | 58.0   | 7.05  | 41.2   | 1.74   |                        |
|                 | Zone E      | 35.0  | 27.5  | 47.5  | 20.0  | 17.5  | 25.0  | 37.5  | 40.0  | 60.0   | 7.50  | 42.5   | 1.00   |                        |
|                 | Scaling     | 1.11  | 0.11  | 2.51  | 12.3  | 7.84  | 0.03  | 5.61  | 25.5  | 66.1   | 0.39  | 1.81   | 0.18   |                        |
| Migration rate  | Zone A      | 0.05  | 0.01  | 0.02  | -0.16 | -0.53 | -0.22 | 0.00  | 0.01  | -0.58  | 0.73  | 0.00   | 45.0   |                        |
|                 | Zone B      | 0.17  | 0.12  | 0.01  | 0.22  | -0.16 | -0.06 | 0.09  | -0.05 | 0.07   | 0.21  | -0.08  | 15.2   |                        |
|                 | Zone C      | -0.19 | 0.05  | 0.00  | 0.16  | -0.08 | -0.01 | 0.02  | -0.06 | -0.27  | 1.40  | -0.04  | 3.14   |                        |
|                 | Zone D      | 0.04  | -0.03 | 0.02  | -0.05 | -0.10 | -0.01 | -0.04 | -0.06 | -0.09  | -0.11 | -0.08  | 0.64   |                        |

Note: “-” means move out; vice versa for move in.

**Table 3.** Rare element content ( $\times 10^{-6}$ ) and data processing results of ore-fresh rock zoning rocks in the Zhangjiawu uranium deposit, Zhejiang Province, China.

|                 | Sub-Banding | La    | Ce    | Pr    | Nd    | Sm    | Eu   | Gd    | Tb    | Dy    | Ho    | Er    | Tm   | Yb   | Lu   | Standardization Factor |
|-----------------|-------------|-------|-------|-------|-------|-------|------|-------|-------|-------|-------|-------|------|------|------|------------------------|
| Raw data        | Zone A      | 50.9  | 91.6  | 10.4  | 37.3  | 6.91  | 1.07 | 5.78  | 0.87  | 4.79  | 1.01  | 3.48  | 0.53 | 3.64 | 0.55 | 1.00                   |
|                 | Zone B      | 50.1  | 93.2  | 10.1  | 36.4  | 6.88  | 1.20 | 5.87  | 0.95  | 5.74  | 1.14  | 3.87  | 0.57 | 3.72 | 0.56 | 1.04                   |
|                 | Zone C      | 16.8  | 75.3  | 4.27  | 15.7  | 3.37  | 0.49 | 3.22  | 0.58  | 3.90  | 0.81  | 2.65  | 0.44 | 3.06 | 0.45 | 1.05                   |
|                 | Zone D      | 35.4  | 86.3  | 7.45  | 26.5  | 5.44  | 0.79 | 4.59  | 0.78  | 4.98  | 1.01  | 3.53  | 0.54 | 3.68 | 0.54 | 1.00                   |
|                 | Zone E      | 52.3  | 104   | 11.6  | 43.1  | 9.51  | 0.40 | 5.24  | 0.82  | 4.74  | 0.97  | 2.71  | 0.41 | 2.62 | 0.39 |                        |
| Standardization | Zone A      | 50.9  | 91.6  | 10.4  | 37.3  | 6.91  | 1.07 | 5.78  | 0.87  | 4.79  | 1.01  | 3.48  | 0.53 | 3.64 | 0.55 |                        |
|                 | Zone B      | 52.2  | 97.0  | 10.5  | 37.9  | 7.16  | 1.25 | 6.11  | 0.99  | 5.98  | 1.19  | 4.03  | 0.59 | 3.87 | 0.58 |                        |
|                 | Zone C      | 17.6  | 78.9  | 4.47  | 16.5  | 3.53  | 0.51 | 3.37  | 0.60  | 4.08  | 0.84  | 2.77  | 0.46 | 3.20 | 0.47 |                        |
|                 | Zone D      | 35.4  | 86.3  | 7.45  | 26.5  | 5.44  | 0.79 | 4.59  | 0.78  | 4.98  | 1.01  | 3.53  | 0.54 | 3.68 | 0.54 |                        |
| Projection data | Zone A      | 21.9  | 43.8  | 28.9  | 17.2  | 29.0  | 80.6 | 27.6  | 47.8  | 27.8  | 15.6  | 44.9  | 13.0 | 24.3 | 38.8 |                        |
|                 | Zone B      | 22.4  | 46.4  | 29.5  | 17.5  | 30.1  | 94.2 | 29.1  | 54.4  | 34.6  | 18.3  | 52.1  | 14.4 | 25.8 | 40.7 |                        |
|                 | Zone C      | 7.59  | 37.7  | 12.4  | 7.66  | 14.8  | 38.8 | 16.1  | 33.2  | 23.6  | 13.0  | 35.8  | 11.2 | 21.3 | 32.8 |                        |
|                 | Zone D      | 15.2  | 41.3  | 20.7  | 12.3  | 22.8  | 59.4 | 21.9  | 43.1  | 28.8  | 15.5  | 45.6  | 13.1 | 24.5 | 37.6 |                        |
|                 | Zone E      | 22.5  | 50.0  | 32.5  | 20.0  | 40.0  | 30.0 | 25.0  | 45.0  | 27.5  | 15.0  | 35.0  | 10.0 | 17.5 | 27.5 |                        |
|                 | Scaling     | 0.43  | 0.48  | 2.79  | 0.46  | 4.21  | 75.5 | 4.77  | 55.0  | 5.80  | 15.4  | 12.9  | 24.5 | 6.68 | 70.0 |                        |
| Migration rate  | Zone A      | -0.08 | -0.17 | -0.16 | -0.18 | -0.31 | 1.55 | 0.05  | 0.01  | -0.04 | -0.01 | 0.22  | 0.24 | 0.32 | 0.34 |                        |
|                 | Zone B      | -0.05 | -0.11 | -0.13 | -0.16 | -0.28 | 1.99 | 0.11  | 0.15  | 0.20  | 0.17  | 0.42  | 0.38 | 0.41 | 0.41 |                        |
|                 | Zone C      | -0.68 | -0.28 | -0.64 | -0.64 | -0.65 | 0.23 | -0.39 | -0.30 | -0.18 | -0.17 | -0.02 | 0.08 | 0.16 | 0.14 |                        |
|                 | Zone D      | -0.36 | -0.22 | -0.40 | -0.42 | -0.46 | 0.87 | -0.17 | -0.10 | -0.01 | -0.03 | 0.23  | 0.24 | 0.32 | 0.29 |                        |

Note: “-” means move out; vice versa for move in.

**Table 4.** Characteristic values of major, trace and rare earth elements of ores-fresh rocks in each zoning of Zhangjiawu uranium deposit ( $\times 10^{-6}$ ).

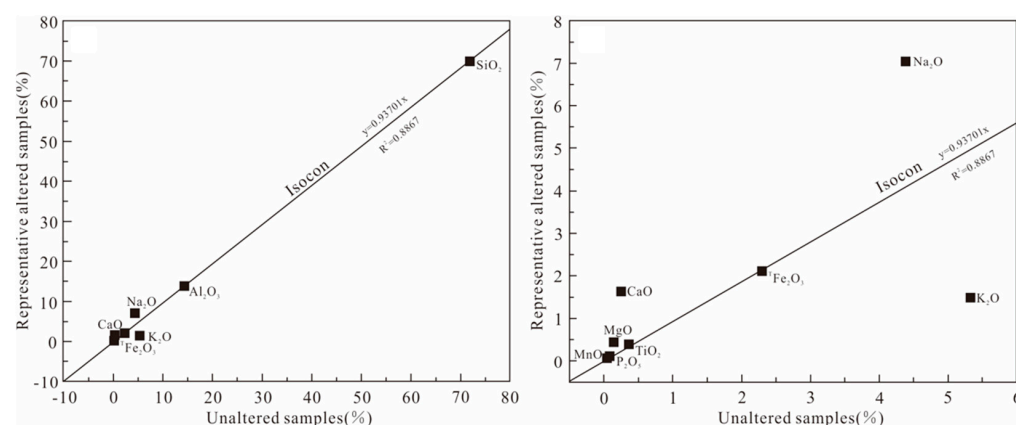
| Sub-Banding          | Zone A | Zone B | Zone C | Zone D | Zone E |
|----------------------|--------|--------|--------|--------|--------|
| OI                   | 0.81   | 0.87   | 0.98   | 0.98   | 0.69   |
| Th/U                 | 0.09   | 0.23   | 0.96   | 2.31   | 4.13   |
| Sm/Nd                | 0.19   | 0.19   | 0.21   | 0.20   | 0.22   |
| $\Sigma$ REE         | 219    | 220    | 131    | 181    | 239    |
| LREE                 | 198    | 198    | 116    | 162    | 221    |
| HREE                 | 20.6   | 22.4   | 15.1   | 19.6   | 17.8   |
| LREE/HREE            | 9.60   | 8.84   | 7.69   | 8.25   | 12.3   |
| (La/Yb) <sub>N</sub> | 10.0   | 9.68   | 3.96   | 6.91   | 14.3   |
| $\delta$ Eu          | 0.52   | 0.58   | 0.46   | 0.48   | 0.17   |
| $\delta$ Ce          | 0.98   | 1.01   | 2.18   | 1.30   | 1.04   |

#### 4. Mass Balance Calculations and Elemental Migration Characteristics

##### 4.1. Standardized Isocon Diagramming Method

The key to mass balance calculations is the determination of the inactive components [23], which is usually achieved using the graphical method proposed by Grant [16]. This suggests that during the opening of the system, the inactive components exhibit the same degree of migration among themselves, and when performing an Isocon graphical cast, a straight line through the origin, the Isocon curve, can be fitted, with the inactive components falling on this curve.

In this paper, the above method was used to determine the inactive fraction. The Isocon curve fitted to the inactive component discrimination diagram (Figure 5) is  $y = 0.93701x$  with a fit  $R^2 = 0.8867$ . It can be seen in Figure 5 that the components falling on the Isocon curve are  $\text{SiO}_2$ ,  $\text{Al}_2\text{O}_3$ ,  $^{\text{T}}\text{Fe}_2\text{O}_3$ ,  $\text{TiO}_2$ ,  $\text{P}_2\text{O}_5$  and  $\text{MnO}$ , indicating that these components may be inactive. Gresens [24] and Grant [16] suggested that Al, Ti, Hf, Th and Zr are usually inactive during hydrothermal alteration. In the Zhangjiawu uranium deposit, silicification, hematite, pyrite, chlorite and sericite are seen, so  $\text{SiO}_2$ ,  $\text{Al}_2\text{O}_3$ ,  $^{\text{T}}\text{Fe}_2\text{O}_3$  are considered to be the active components. In the process of hydrothermal uranium mineralization, apatite is closely related to uranium mineralization, and uranium minerals are closely related to apatite in Zhangjiawu uranium deposit, so  $\text{P}_2\text{O}_5$  is considered the active component. The Zhangjiawu uranium deposit is of medium–low temperature hydrothermal origin, the relationship between Ti and uranium mineralization is not close and the content of  $\text{MnO}$  is less in the system than elsewhere. In summary,  $\text{TiO}_2$  was identified as the inactive component for the mass balance calculation.

**Figure 5.** Diagrams for discriminated immobile elements and Isocon curves.

#### 4.2. Elemental Migration Characteristics

See Table 1 for major element data processing method, Figure 5 for standardized Isocon diagrams and Table 2 for trace element characteristic value calculations. Hydrothermal altered rocks and ores (zone A to D) show an overall decrease in  $\text{SiO}_2$ , FeO and  $\text{K}_2\text{O}$  to varying degrees compared with fresh rocks (zone E) (Table 1, Figure 6A); the contents of  $^{\text{T}}\text{Fe}_2\text{O}_3$ , MgO, CaO,  $\text{Na}_2\text{O}$  and loss on ignition (LOI) increased to different degrees. The contents of  $\text{TiO}_2$ ,  $\text{Al}_2\text{O}_3$ , MnO and  $\text{P}_2\text{O}_5$  increased slightly. Fresh rock (E) ~ uranium ore (A). In Figure 6A, FeO and  $^{\text{T}}\text{Fe}_2\text{O}_3$ ,  $\text{K}_2\text{O}$  and  $\text{Na}_2\text{O}$  show an inverse proportional relationship. The increase in  $^{\text{T}}\text{Fe}_2\text{O}_3$ , CaO and  $\text{Na}_2\text{O}$  in altered rocks corresponds to the hematite, calcite and sodic feldspar mineralization in the surrounding rocks; the oxidation index (OI) becomes higher and the LOI increases significantly from fresh rock to ore, ranging from 0.69 to 0.98 and 0.59% to 3.1%, respectively. This indicates that the mineralized hydrothermal fluid has high levels of oxygen escaping and is rich in volatiles and mineralizing agents [23]. The standardized Isocon curves (Figure 6B) and migration rates (Table 1) of the main elements show that the main elements migrated in more than out during hydrothermal alteration overall, with  $^{\text{T}}\text{Fe}_2\text{O}_3$ , CaO,  $\text{Na}_2\text{O}$ ,  $\text{P}_2\text{O}_5$  and LOI showing significant migration in, FeO and  $\text{K}_2\text{O}$  showing significant migration out, and  $\text{Al}_2\text{O}_3$  and  $\text{SiO}_2$  showing no significant migration in or out. In the central zone of mineralization, CaO,  $\text{Na}_2\text{O}$ , MgO and  $\text{P}_2\text{O}_5$  were clearly migrating in and  $\text{K}_2\text{O}$  was clearly migrating out, suggesting that the enrichment of mineralized elements in the Zhangjiawu uranium deposit is related to the gain of CaO, MgO,  $\text{Na}_2\text{O}$ ,  $\text{P}_2\text{O}_5$  and the loss of  $\text{K}_2\text{O}$ .

As can be seen from the trace element primitive mantle standardized spider web diagram (Figure 7A), the fresh rocks, altered rocks and ores show similar trace element compositional characteristics, with a few elements being highly variable, suggesting that the trace elements are relatively stable and that the mineralizing fluids may not have had multiple sources. All zoned rocks are enriched in the macroionic lithophile elements Rb, Th and U, deficient in Ba and Sr, and with little variation in the high field strength elements Nb, Ta, Zr, and Hf. Compared with fresh rocks, altered rocks are more enriched in U, and the higher the degree of alteration, the greater the enrichment; the variation in Th is relatively small, but the corresponding Th/U value decreases with increasing alteration ( $4.13 \times 10^{-6} \rightarrow 0.09 \times 10^{-6}$ ) for fresh rocks  $\rightarrow$  distal altered rocks  $\rightarrow$  near-mineral altered rocks  $\rightarrow$  paragenetic altered rocks  $\rightarrow$  ore, indicating a continuous enrichment of U had occurred. From the standardized Isocon diagram of trace elements (Figure 7B) and the mobility characteristics (Table 3), it can be seen that alteration zone rocks gain U, Pb, Cu, Zn, Co and Cr to various degrees, and lose Li, V, Ba, Sr, Ni, Rb and Tl to various degrees compared with fresh rocks, while Nb, Ta, Zr and Hf do not show significant transfer. In the central zone of mineralization (ore), U, Zn and Co transfer in significantly, Cu and Pb to a lesser extent, and Cs, Rb and Tl transfer out significantly, indicating that uranium mineralization is closely related to the gain of Zn, Co, Cu and Pb and the loss of Cs, Rb and Tl, indicating that the uranium mineralizing fluids are enrichment for chalcophile elements.

As can be seen from the chondrite normalized REE pattern diagram (Figure 8A), the fresh rocks, altered rocks and ores show similar rare earth distribution patterns with relatively consistent trends, suggesting that there may not be multiple sources of mineralizing fluids and that alteration has less influence on the rare earth distribution patterns of the rocks in each zone. Compared to fresh rocks, the total rare earths ( $\Sigma\text{REE}$ ), light REEs (LREEs), the LREE to heavy REE (HREE) ratio and  $(\text{La}/\text{Yb})_{\text{N}}$  equivalents all decrease and the HREE content increases (Table 3), suggesting that the fractionation of light and heavy elements is somewhat reduced. The greater increase in  $\delta\text{Eu}$  values in altered rocks may indicate the formation of plagioclase feldspar during alteration. In the standardized Isocon diagram of the REEs (Figure 8B), the LREEs such as La, Ce, Pr, Nd and Sm show a greater degree of migration out, while Eu and most of the HREEs such as Tm, Er, Yb and Lu show a greater degree of gain, with reduced fractionation of LREEs and HREEs during alteration. The results suggest that uranium mineralization is closely related to the transfer of HREEs.

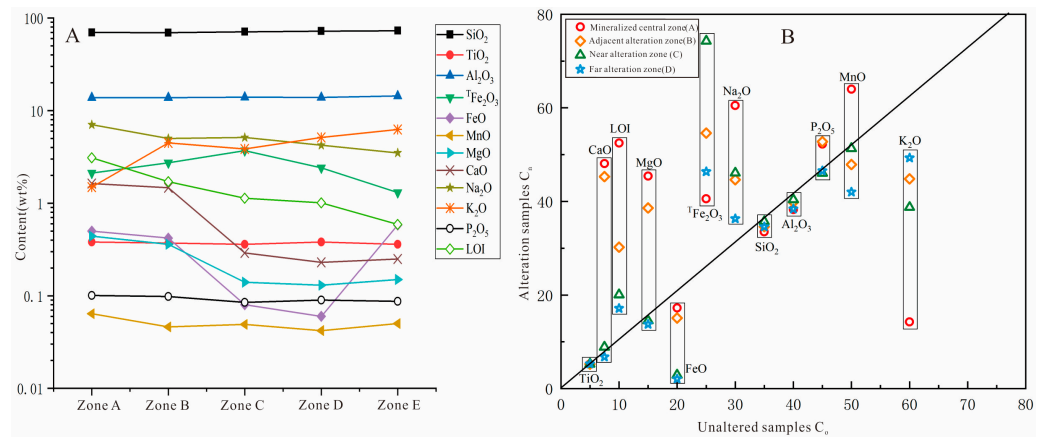


Figure 6. (A) Content and (B) standardized Isocon diagram of major elements.

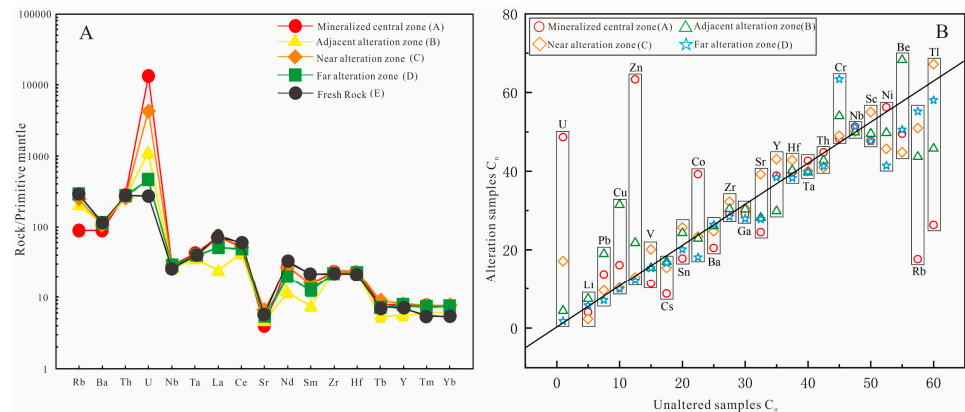


Figure 7. (A) Primitive mantle-normalized trace element spider diagram (normalization values after ref. [24]) and (B) standardized Isocon diagram for trace elements.

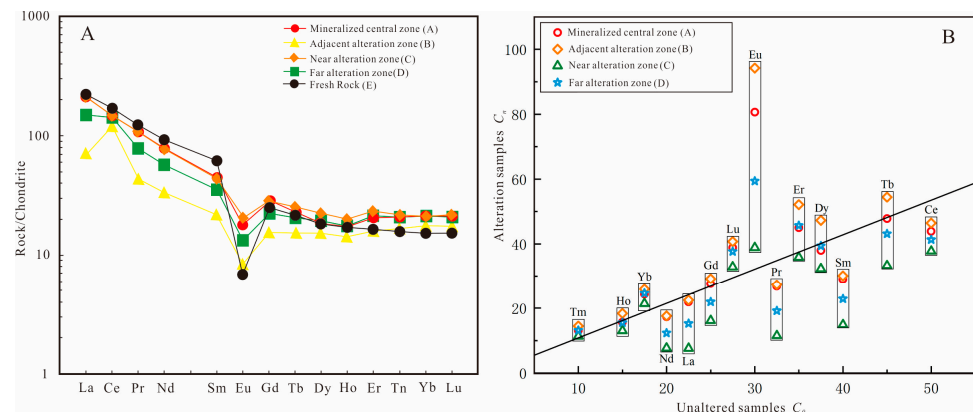


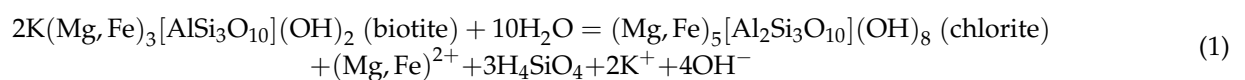
Figure 8. (A) chondrite normalized REE pattern diagram (normalization values after ref. [24]) and (B) standardized Isocon diagram for REE.

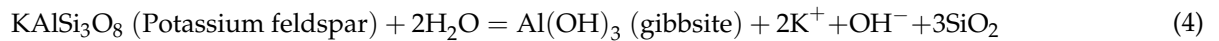
## 5. Discussion

### 5.1. Elemental Migration Patterns and Mechanisms

During alkali metasomatism, monovalent and polyvalent metal ions are usually substituted in order to maintain the electric charge balance of the rock, while divalent alkaline earth element ions are brought out [25]. During hydrothermal alteration of the Zhangjiawu uranium deposit, CaO migration is evident in the alteration zone next to the mine and in the central zone of mineralization, as evidenced by strong calcitization (carbonation;

Figure 4c,e,f). This paper shows that uranium in the Zhangjiawu uranium deposit has mainly migrated as uranyl carbonate complexes ( $[\text{UO}_2(\text{CO}_3)_2]^{2-}$   $[\text{UO}_2(\text{CO}_3)_3]^{4-}$ ), and the substitution of  $\text{Ca}^{2+}$  in the alteration zone next to the mine and in the central zone of mineralization causes a decrease in the activity of  $\text{CO}_3^{2-}$ , which promotes the precipitation of uranium;  $\text{CaO}$  is migrated out the near and far alteration zones, probably to maintain the rock electrovalence balance. The migration degree of  $\text{Fe}_2\text{O}_3$  in the mineralization center and near ore alteration zone is weaker than that in near and far ore alteration zones, which may be related to the large-scale oxidation in the early stage of mineralization and the small reduction in the late stage of mineralization. In addition,  $\text{FeO}$  migrated out in all zones, indicating that it may be related to hematite (conversion of  $\text{FeO}$  to  $\text{Fe}_2\text{O}_3$ ), biotite greenification (Equation (1)) and the electric charge balance during the alteration process. The essence of uranium precipitation is the reduction of  $\text{U}^{6+}$  to  $\text{U}^{4+}$ , and the transition from an oxidizing to a reducing environment in the mineralized central zone promotes uranium precipitation. Meanwhile,  $\text{K}_2\text{O}$  migrated out in all zones, and the degree of transfer increased alteration. The gain in  $\text{Na}_2\text{O}$  was observed in all zones, and this increased with increasing alteration. An inverse relationship exists between  $\text{K}_2\text{O}$  and  $\text{Na}_2\text{O}$ , which is manifested as potassium feldspar metasomatized by alfeldspar in different zones (Figure 4). In the process of sodium metasomatism,  $\text{K}^+$  with larger ionic radius ( $1.33 \times 10^{-10}$  m) is replaced by  $\text{Na}^+$  with smaller radius ( $0.98 \times 10^{-10}$  m), which reduces the volume of feldspar cells. As a result, the porosity of sodium metasomatic rock is increased or micro-fractures are easily generated under the action of stress, providing favorable conditions for mineralization. In addition, this phenomenon may be related to the sericitization (Equation (2)) and clayification (Equation (3)) of potassium feldspar. Meanwhile,  $\text{MgO}$  is migrating in the central and paragenetic alteration zones, causing a decrease in the  $\text{CO}_3^{2-}$  activity and promoting uranium precipitation. At the same time,  $\text{MnO}$  shows migration within the near, far and paragenetic alteration zones and migration in the central zone of mineralization, which is often explained by convective equilibrium migration of elements [23,26]. Migration of  $\text{P}_2\text{O}_5$  occurs in the central and paragenetic alteration zones of mineralization, which may be related to the formation of contained paragenetic minerals. The migration of phosphorus (usually considered a deep source near the mantle) indicates that the uranium source or ore-forming fluid is of deep origin. The near and far ore alteration zones are basically stable, without obvious migration in and out. The LOI shows migration in all zones, from fresh rock  $\rightarrow$  distal alteration zone  $\rightarrow$  near-mine alteration zone  $\rightarrow$  paragenetic alteration zone  $\rightarrow$  central zone of mineralization, with increasing migration, indicating that the increasing alteration of the rock is related to the formation of water-bearing paragenetic minerals and fluid-bearing volatile matter formed by alteration. In addition,  $\text{Al}_2\text{O}_3$  and  $\text{SiO}_2$  show migration in all zones, with increasing migration from the distal alteration zone to the center of mineralization, but overall migration is low; the migration of  $\text{Al}_2\text{O}_3$  can be explained by the decomposition of feldspar (Equation (4));  $\text{SiO}_2$  shows migration out, but microcrystalline quartz and chalcedony are seen in altered rocks, often as vein-filling in bulk specimens as a product of late mineralization. The results of the late mineralization are often vein filled in bulk specimens. The solubility of  $\text{SiO}_2$  has been shown to increase with increasing temperature and pH [25], which provides a good explanation for the migration characteristics of  $\text{SiO}_2$  and reflects the trend of decreasing temperature and pH during alteration. The reactions related to the hydrothermal alteration process [15,23,25,27] are presented below:





During hydrothermal alteration, ion exchange between hydrothermal fluids and minerals along with the decomposition of trace element-bearing minerals in rocks results in the activation of elemental migration [26,28]. Ion exchange depends on the diffusion rate of elements in minerals, but the diffusion rate of elements in minerals is very slow. Therefore, the main cause of the activation of trace element migration is the decomposition of trace element-containing minerals [23,26,29]. For example, Rb, Cs and K have the same ionic radius and show similar geochemical properties, and all three co-exist in K-bearing potassium feldspar and mica [29]. The elements Rb, Cs and K show migration in each alteration zone, which can be explained by the sodium feldspar accounting for potassium feldspar, with a higher degree of alteration in the center of the mineralization showing a strong migration of these three elements. The significant migration in of Cu, Pb and Zn in the mineralized central and near-mineralized alteration zones indicates that the hydrothermal fluids are enriched in Cu, Pb and Zn, which corresponds to the precipitation of sphalerite and galena during hydrothermal alteration and also to the regional (within the Hu-An basin) Pb-Zn polymetallic mineralization after ~137 Ma [26,30,31], suggesting that the Zhangjiawu area has potential for uranium-polymetallic mineralization. Meanwhile, U is substituted in all alteration zones, with the substitution rate ranging from the distal alteration zone (0.64) to the center of mineralization (45.08) reflecting a high enrichment of U and indicating a hydrothermal-rich uranium source.

The REEs are less abundant in the main rock-forming minerals; they are mainly contained in in paragenetic minerals [23]. Therefore, the activation of migration in REEs in alteration zones is not dominated by the decomposition/crystallization of REE-bearing minerals, but by magmatic-hydrothermal interaction [32]. The migration of LREEs and HREEs in all alteration zones is due to the similar geochemistry of HREEs and U, which are easily migrated by complexes in hydrothermal fluids rich in  $\text{HCO}_3^-$ ,  $\text{CO}_3^{2-}$  and  $\text{F}^-$  ions, while LREEs exhibit strong adsorption capacity [23] and are continuously reduced by the adsorption of alteration minerals during fluid transport.

### 5.2. Hydrothermal Alteration and Mineralization Mechanisms

The study of hydrothermal alteration at the Zhangjiawu uranium mine is important for understanding the source of ore-forming material, the migration mechanism of uranium and the precipitation of uranium. The migration characteristics of REEs in altered rocks show a significant migration of HREEs, and the enrichment of HREEs reflects the deep source origin of the mineralizing fluids [28,33–37]; Sm/Nd values of 0.19 to 0.21 (Table 1) within each alteration zone are less than 0.35, indicating a mantle origin [38–41]. The migration of  $\text{P}_2\text{O}_5$  into the central zone of mineralization and the alteration zone adjacent to the mine is also indicative of a deep source of mineralizing fluids. The consistency of the REE partitioning patterns and trace element spider web diagrams of altered and fresh rocks suggest that the fluids may be consistent with a source of the parent magma, being the product of partial melting of the magnesium-iron subcrust. The mantle fluids are characterized by low oxygen fugacity [42,43], which is not sufficient to form the high oxygen fugacity conditions required for  $\text{U}^{6+}$  migration. The OI values of the alteration samples ranged from 0.81 to 0.98 (the lowest in the central zone of mineralization), indicating that the fluids were characterized by high oxygen fugacity during mineralization. In summary, this paper suggests that the mineralizing fluid may be a mixture of partially molten deep source fluids from the lower crust and deep circulation atmospheric precipitation, and that the strong tensional environment after the formation of the Zhangjiawu ore-bearing rhyolite (130 Ma) provided the potential for fluid mixing.

Sodium feldspar accounts for potassium feldspar resulting in increased porosity of sodium-metasomatism in rocks, leading to easy formation of microfractures under stress, which in turn provides space conducive to uranium migration/enrichment. The essence of uranium precipitation is the reduction of  $\text{U}^{6+}$  to  $\text{U}^{4+}$ , and uranium in the Zhangji-

awu uranium deposit is mainly migrated as uranyl carbonate complexes ( $[\text{UO}_2(\text{CO}_3)_2]^{2-}$ ,  $[\text{UO}_2(\text{CO}_3)_3]^{4-}$ ). Additionally, the substitution of  $\text{Ca}^{2+}$ , and  $\text{Mg}^{2+}$  within the alteration zone next to the mine and the central zone of mineralization causes a decrease in the activity of  $\text{CO}_3^{2-}$ , promoting uranium precipitation; the migration pattern of  $\text{FeO}$  and  $\text{Fe}_2\text{O}_3$  reflects the change from oxidizing to reducing conditions in the central zone of mineralization. The transferring of  $\text{SiO}_2$  reflects the decrease in temperature and pH during mineralization, recording a shift from hydrothermal alteration to a physicochemical environment (neutral to weak alkaline) favorable for uranium precipitation.

## 6. Conclusions

- (1) The alteration of the surrounding rocks of the Zhangjiawu uranium mine is well developed, with the main types of alteration being hematite, sodic feldspar, chlorite, mud, and carbonate, with obvious alteration zoning, of which hematite is most closely related to uranium mineralization.
- (2) Studies on the hydrothermal alteration characteristics of the Zhangjiawu uranium deposit indicate that  $\text{CaO}$ ,  $\text{MgO}$ ,  $\text{Na}_2\text{O}$ ,  $\text{P}_2\text{O}_5$ ,  $\text{LOI}$ ,  $\text{Zn}$ ,  $\text{Co}$ ,  $\text{Cu}$ ,  $\text{Pb}$  and HREEs show migration in, and  $\text{K}_2\text{O}$ ,  $\text{Cs}$ ,  $\text{Rb}$  and  $\text{Tl}$  show migration out during uranium mineralization, which is consistent with the development of hematite, sodic feldspar and carbonation in the ore zone. In addition,  $\text{MnO}$  and  $\text{MgO}$  show a negative correlation in the alteration zone, indicating a possible elemental convective equilibrium migration pattern in the mine area.
- (3) Studies on the migration mechanism of elements indicate that the migration of  $\text{P}_2\text{O}_5$  and HREE is indicative of the deep source nature of the mineralizing fluids; the migration of  $\text{Zn}$ ,  $\text{Co}$ ,  $\text{Cu}$  and  $\text{Pb}$  is indicative of metal-rich fluids; alteration can lead to a reduction in the activity of uranyl complexes, the formation of a reducing environment and a neutral to weak alkaline environment favorable for uranium precipitation, leading to uranium precipitation and mineralization.

**Author Contributions:** Conceptualization, W.Z. and Z.C.; methodology, W.Z. and B.W.; formal analysis, Y.T. and W.L.; investigation, X.L. and Z.X.; writing—original draft preparation, W.Z. and B.W.; writing—review and editing, X.W. and Z.C. All authors have read and agreed to the published version of the manuscript.

**Funding:** This research was jointly supported by the National Natural Science Foundation of China (Grants: 41902214, 42172258), the CGS Research Fund (Grants: DZLXJK201904), the China Geological Survey (Grants: DD20190161, DD20221660-3), State Key Laboratory for Mineral Deposits Research (2020-LAMD-K03) and Joint Innovation Fund of China National Uranium Co., Ltd. and State Key Laboratory of Nuclear Resources and Environment (No. NRE2021-01).

**Data Availability Statement:** The original contributions presented in the study are included in the article. Further inquiries can be directed to the corresponding author.

**Acknowledgments:** We would like to thank No. 262 Geological Party of Zhejiang Nuclear Industry Corp. We also thank Xiaowei Zheng and Huanyuan Chen for his help in the field works.

**Conflicts of Interest:** The authors declare that the research was conducted in the absence of any commercial or financial relationships that could be construed as a potential conflict of interest.

## References

1. Pirajno, F. Hydrothermal processes and wall rock alteration. In *Hydrothermal Processes and Mineral Systems*; Springer: Dordrecht, The Netherlands, 2009; pp. 73–164.
2. Guo, S.; Ye, K.; Chen, Y.; Liu, J.B. A normalization solution to mass transfer illustration of multiple progressively altered samples using the isocon diagram. *Econ. Geol.* **2009**, *104*, 881–886. [[CrossRef](#)]
3. Guo, S.; Ye, K.; Chen, Y.; Liu, J.B.; Zhang, L.M. Introduction of mass-balance calculation method for component transfer during the opening of a geological system. *Acta Petrol. Sin.* **2013**, *29*, 1486–1498, (In Chinese with English abstract).
4. Bogossian, J.; Hagemann, S.G.; Rodrigues, V.G.; Lobato, L.M.; Roberts, M. Hydrothermal alteration and mineralization in the Faina greenstone belt: Evidence from the Cascavel and Sertão orogenic gold deposits. *Ore Geol. Rev.* **2020**, *119*, 103293. [[CrossRef](#)]

5. Gaillard, N.; Williams-Jones, A.E.; Clark, J.R.; Lypaczewski, P.; Salvi, S.; Perrouty, S.; Linnen, R.L. Mica composition as a vector to gold mineralization: Deciphering hydrothermal and metamorphic effects in the Malartic district, Quebec. *Ore Geol. Rev.* **2018**, *95*, 789–820. [[CrossRef](#)]
6. Gao, S.; Xu, H.; Li, S.; Santosh, M.; Zhang, D.; Yang, L.; Quan, S. Hydrothermal alteration and ore-forming fluids associated with gold-tellurium mineralization in the Dongping gold deposit, China. *Ore Geol. Rev.* **2017**, *80*, 166–184. [[CrossRef](#)]
7. Harris, A.C.; Golding, S.D. New evidence of magmatic-fluid-related phyllic alteration: Implications for the genesis of porphyry Cu deposits. *Geology* **2002**, *30*, 335–338. [[CrossRef](#)]
8. Xu, W.G.; Fan, H.R.; Yang, K.F.; Hu, F.F.; Cai, Y.C.; Wen, B.J. Exhaustive gold mineralizing processes of the Sanshandao gold deposit, Jiaodong Peninsula, eastern China: Displayed by hydrothermal alteration modeling. *J. Asian Earth Sci.* **2016**, *129*, 152–169. [[CrossRef](#)]
9. Akella, J. Calculation of material transport in some metasomatic processes. *Neues Jahrb. Mineral.-Abh.* **1966**, *104*, 316–329.
10. Gresens, R.L. Composition-volume relationships of metasomatism. *Chem. Geol.* **1967**, *2*, 47–55. [[CrossRef](#)]
11. Grant, J.A. The isocon diagram: A simple solution to gresensequation for metasomatic alteration. *Econ. Geol.* **1986**, *81*, 1976–1982. [[CrossRef](#)]
12. Ague, J.J. Mass transfer during Barrovian metamorphism of pelites, South-Central Connecticut. 1. Evidence for changes in composition and volume. *Am. J. Sci.* **1994**, *294*, 989–1057. [[CrossRef](#)]
13. Liu, R.R.; Li, Z.Y.; Tang, J.W.; Xu, X.Q. The source of uranium metallogenic fluid and its migration and enrichment mechanism in Quzhou area, Zhejiang. *J. East China Univ. Technol.* **2018**, *41*, 101–110.
14. Xu, Z.H. *Ore-Controlling Structure and Metallogenic Prediction of Zhangjiawu Uranium Deposit in Moganshan Volcanic Basin, Northern Zhejiang Province*; China University of Geosciences: Wuhan, China, 2020.
15. Wang, B.; Zhang, W.G.; Chen, Z.L.; Pan, J.Y.; Xu, Z.H.; Liu, X. A study on ore characteristics and uranium occurrence state of the Zhangjiawu uranium deposit in the northern Zhejiang, China. *Acta Mineral. Sin.* **2022**, *42*, 40–50.
16. Yang, L.; Yu, L.; Liu, K.; Jia, J.; Zhu, G.; Liu, Q. Coupled effects of temperature and solution compositions on metasomatic dolomitization: Significance and implication for the formation mechanism of carbonate reservoir. *J. Hydrol.* **2022**, *604*, 127199. [[CrossRef](#)]
17. Fang, X.H.; Fang, M.L.; Luo, Y. The potential evaluation of volcanic type uranium resources in China. *Uranium Geol.* **2012**, *28*, 342–348, 354.
18. Wu, J.H.; Guo, G.L.; Guo, J.L.; Zhang, Q.; Wu, R.G.; Yu, D.G. Spatial-temporal distribution of Mesozoic igneous rock and their relationship with hydrothermal uranium deposits in eastern China. *Acta Petrol. Sin.* **2017**, *33*, 1591–1614.
19. Zhang, J.D.; Guo, Q.Y.; Li, Y.L.; Li, Z.Y.; Cai, Y.Q.; Han, C.Q. The main advance and achievements in the potential evaluation of uranium resource in China. *Uranium Geol.* **2012**, *28*, 321–326.
20. Ma, F.; Xue, H.M. Huzhou-Anji volcanic basin of north Zhejiang Province: Zircon U-Pb dating, geochemistry and magma genesis. *Acta Geol. Sin.* **2017**, *91*, 334–361.
21. Tang, Z.C.; Meng, X.S.; Dong, X.F.; Wu, X.Y.; Chen, Z.D.; Yu, S.Q.; Zhao, X.D. Zircon U-Pb Ages and Hf Isotopic Compositions of the Late Mesozoic Intrusive Rocks in Northern Zhejiang: Implications for Genetic Evolution and Tectonic Environment. *Geotecton. Metallog.* **2018**, *42*, 403–419.
22. Yan, Q.J.; Zhang, W.G.; Chen, Z.L.; Wang, X.H.; Xu, Z.H.; Liu, X.; Ding, Z.L.; Wang, B. Granite Denudation Degree and Its Implications for Fluorite Prospecting in Hu'an Area, Northwest Zhejiang Province: Evidence from Apatite Fission Track Thermochronology. *Acta Petrol. Sin.* **2021**, *42*, 651–662.
23. Wu, D.H.; Xia, F.; Pan, J.Y.; Liu, G.Q.; Huang, G.L.; Liu, W.Q.; Wu, J.Y. Characteristics of hydrothermal alteration and material migration of Mianhuakeng uranium deposit in northern Guangdong Province. *Acta Petrol. Sin.* **2019**, *35*, 2745–2764.
24. Zhang, W.-F.; Xia, X.-P.; Su, B.-X.; Xu, Y.-G.; Zhang, Y.-Q.; Yang, Q.; Zhang, L.; Cui, Z.-X. Distinct Geochemical Behavior of Water in Olivine between Silicate and Carbonatite Metasomatism. *Minerals* **2022**, *12*, 1090. [[CrossRef](#)]
25. Yu, D. Prospecting ideas for mesozoic granite-type, volcanics-type and exo-contact-type uranium deposits in South China—Part 1. *Uranium Geol.* **2001**, *17*, 257–265.
26. Li, H.D.; Pan, J.Y.; Xia, F.; Zhou, J.Y.; Liu, Y.; Zhong, F.J. Hydrothermal alteration and its geochemical characteristics of Lijialing deposit in Xiangshan uranium ore deposit. *Geoscience* **2016**, *30*, 555–566.
27. Yu, D. Prospecting ideas for mesozoic granite-type, volcanic-type, exo-contact-type uranium deposits in South China—Part 2. *Uranium Geol.* **2001**, *17*, 321–327.
28. Du, L.T. *Basic Metallogenic Regularity and General Hydrothermal Metallogeny of Hydrothermal Uranium Deposits in China*; Beijing Atomic Energy Press: Beijing, China, 2001; pp. 1–307.
29. Campbell, I.H.; Lesher, C.M.; Coad, P.; Franklin, J.M.; Gorton, M.P.; Thurston, P.C. Rare-earth element mobility in alteration pipes below massive Cu Zn-sulfide deposits. *Chem. Geol.* **1984**, *45*, 181–202. [[CrossRef](#)]
30. Xie, Y.L.; Tang, Y.W.; Li, Y.X.; Liu, B.S.; Qiu, L.M.; Zhang, X.X.; Jiang, Y.C. Magmatic intrusive series and their implication for the ore prospecting in Anji exploration area, Zhejiang Province. *Acta Petrol. Sin.* **2012**, *28*, 3334–3346.
31. Li, Y.X.; Xie, Y.L.; Tang, Y.W.; Zhang, X.X.; Qiu, L.M. A preliminary study of source of lead in Gangkou polymetallic deposit, Anji, Zhejiang Province: Lead isotope evidence. *Miner. Depos.* **2012**, *31*, 917–929.

32. Wang, C.Y.; Li, X.F.; Xiao, R.; Bai, Y.P.; Yang, F.; Mao, W.; Jiang, S.K. Elements mobilization of mineralized porphyry rocks during hydrothermal alteration at Zhushahong porphyry copper deposit, Dexing district, South China. *Acta Petrol. Sin.* **2012**, *28*, 3869–3886.
33. Wei, B. Adsorption of Rare Earth Elements La, Nd by Clay Minerals Inorganic Elements of Soils. Master's Thesis, Anhui Agricultural University, Anhui, China, 2011; pp. 1–57.
34. Zhang, G.Y.; Wang, S.Z.; Wang, Z.Q.; Liang, L. Correlation of ree features between Xiangshan and Xiazhuang uranium ore fields. *J. East China Inst. Technol.* **2007**, *30*, 9–14.
35. Li, H.; Danišik, M.; Zhou, Z.K.; Jiang, W.C.; Wu, J.H. Integrated U–Pb, Lu–Hf and (U–Th)/He analysis of zircon from the Banxi Sb deposit and its implications for the low-temperature mineralization in South China. *Geosci. Front.* **2020**, *11*, 1323–1335. [[CrossRef](#)]
36. Li, H.; Kong, H.; Guo, B.Y.; Soh Tamehe, L.; Zhang, Q.; Wu, Q.H.; Xi, X.S. Fluid inclusion, H–O–S isotope and rare earth element constraints on the mineralization of the Dong'an Sb deposit, South China. *Ore Geol. Rev.* **2020**, *126*, 103759. [[CrossRef](#)]
37. Li, H.; Palinkaš, L.A.; Evans, N.J.; Watanabe, K. Genesis of the Huangshaping W–Mo–Cu–Pb–Zn deposit, South China: Role of magmatic water, metasomatized fluids, and basinal brines during intra-continental extension. *Geol. J.* **2020**, *55*, 1409–1430. [[CrossRef](#)]
38. Tang, Y.W.; Xie, Y.L.; Li, Y.X.; Qiu, L.M.; Liu, B.S.; Li, Y.; Han, Y.D. Petrogeochemical and petrographic characteristics and genesis of Wushanguan complex body in Anji ore district, Zhejiang Province. *Miner. Depos.* **2012**, *31*, 903–916.
39. Xiao, C.H.; Chen, Z.L.; Liu, X.C.; Wei, C.S.; Wu, Y.; Tang, Y.W.; Wang, X.Y. Structural analysis, mineralogy, and cassiterite U–Pb ages of the Wuxu Sb–Zn–polymetallic district, Danchi Fold-and-Thrust belt, South China. *Ore Geol. Rev.* **2022**, *150*, 105150. [[CrossRef](#)]
40. Xiao, C.H.; Liu, X.H.; Yu, P.P.; Liu, X.C.; Tang, Y.W.; Wang, W.L.; Zhang, Y. Cassiterite U–Pb Dating and Micro-XRF Analysis Constraint on the Formation of Xinlu Sn–Zn Deposit, South China. *Front. Earth Sci.* **2022**, *10*, 1031681. [[CrossRef](#)]
41. Xiao, C.H.; Shen, Y.K.; Wei, C.S.; Su, X.K.; Le, X.W.; Zhang, L. LA-ICP-MS Zircon U–Pb dating, Hf isotopic composition and Ce<sup>4+</sup>/Ce<sup>3+</sup> characteristics of the Yanshanian acid magma in the Xidamingshan cluster, southeastern margin of the Youjiang Fold Belt, Guangxi. *Geoscience* **2018**, *32*, 289–304, (In Chinese with English abstract).
42. Liu, C.Q. The geofluid in the mantle and its role in ore-forming processes. *Earth Sci. Fron.* **2001**, *8*, 231–243.
43. Wang, Z.Q.; Li, Z.Y. Discussion on mantle-derived uranium mineralization. *Geol. Rev.* **2007**, *53*, 608–615.

**Disclaimer/Publisher's Note:** The statements, opinions and data contained in all publications are solely those of the individual author(s) and contributor(s) and not of MDPI and/or the editor(s). MDPI and/or the editor(s) disclaim responsibility for any injury to people or property resulting from any ideas, methods, instructions or products referred to in the content.